The 4th International Symposium on More Electric Aircraft Technology (MEA 2017)

8–9 November 2017

# Research on three-phase four-leg matrix converter based more electric aircraft wing ice protection system

*Songtao Huang[1], Lie Xu[2], Yougui Guo[1], Yongdong Li[2], Wenlang Deng[1]*

[1]*School of Information and Engineering, Xiangtan University, Xiangtan, People's Republic of China*
[2]*State Key Laboratory of Control and Simulation of Power Systems and Generation Equipments, Tsinghua University, Beijing, People's Republic of China*
*E-mail: youguiguo1968@foxmail.com*

Published in *The Journal of Engineering*; Received on 10th January 2018; Accepted on 17th January 2018

**Abstract:** In this study, a new three-phase four-leg matrix converter (TFMC) topology is proposed, and the three-dimensional space vector modulation (3DSVM) strategy is used to realise the output with the three-phase unbalanced load. Aiming at the situation that the icing area of the more electric aircraft on the wing is larger than the icing area in the belly, wing ice protection system is constructed by using the TFMC. Through the real-time detection of the heating element temperature and icing condition by the sensor installed in the wing and belly position, working temperature and three-phase output power of TFMC can be set reasonably. In order to save fuel consumption and reduce operating costs, the key point is to reduce the power transmission in belly position. Finally, simulation and experiment verify the correctness of the proposed 3DSVM strategy and realise the TFMC output with unbalanced three-phase load.

## 1 Introduction

The concept of more electric aircraft (MEA) can be traced back to the period of the Second World War, due to the lack of device manufacturing technology and power electronic converter technology, restricting the application of these concepts until the end of 1970s, when MEA getting the practical application. However, in the aviation field, there will be icing, frost and other phenomena in the wings and abdomen of MEA, which will affect the flight safety [1–4].

For structural in-flight icing, as research in this paper, two necessary conditions included: (i) the plane must pass through visible water, such as rain or clouds of water droplets and (ii) water droplets hitting the aircraft must be at temperatures of 0 °C or colder. It is important to note that aerodynamic cooling can reduce the temperature of the wing surface by several degrees [5, 6]. Supercooled water increases the rate of icing and rapidly accretes. Supercooled water is an unstable state that exists below 0°C in the form of liquid. At 0 and −25°C, most clouds are formed by supercooled water. As the plane passes through these clouds, supercooled water freezes immediately along with wings, fuselage and so on. There are three types: structural icing, clear ice rime and a mixture of the two.

Icing can have bad effects on aircraft flight performance, such as reducing lift and fuel efficiency, increasing resistance, weight and greater power demand. Icing could be hazardous at every flight phase [7].

The existing de-icing system mainly consists of the thermal de-icing system, pneumatic de-icing system and chemical de-icing system. Thermal de-icing is to prevent ice formation on protected aircraft wings and aircraft bellies by the use of electrical heating devices. Another way is to heat the ice by absorbing the heat from an aircraft engine. The pneumatic de-icing system usually consists of inflatable rubber boots at the leading edge of the wing. This kind of rubber boots is inflated with air and causes ice to break and fall off the surface. Another alternative is to use chemicals on the surface of aircraft. Chemicals can be an either dry solid or liquid, having a common characteristic of lowering the freezing point of water. Among them, the method of de-icing by thermal control of ice is most widely used.

More electric system can be used for aircraft propulsion system, electric de-icing system, environmental control and fuel pumping. The Boeing 787 and the Airbus A380 both have a significantly larger multi-electric system. The main advantage of the electrical system is to increase the efficiency of the engine by reducing fuel consumption [8]. The traditional power electronic converter system has DC bus capacitance, in which the electrolytic capacitor has poor reliability and stability, and weak ability to endure ripple current. Thin film capacitors are of large size and weight, low energy density, cannot meet the demand of high power density. The unit price of a capacitor in the large capacity system has been equivalent or exceeds the power electronics. Most importantly, capacitors are prohibited in the high-performance occasions, such as military aerospace.

How to solve it? The three-phase three-leg matrix converter (TFMC) is introduced into the multi-electric system, which has the advantages of small volume, lightweight, high power density and so on. The most important advantage is that the output can bring the unbalanced load. By detecting the ice on the wing and the belly, the power on the three-phase output load is reasonably configured. In this way, the power loss in the aircraft belly is greatly saved, and the operation cost is reduced.

The rest of the paper is organised as follows. In Section 2, the composition and working principle of the multi-electric system on the EMA based on the TFMC are introduced. Section 3 describes how to implement the TFMC output with unbalanced load based on three-dimensional space vector modulation (3DSVM) control strategy. In Section 4, the simulation and experimental results are given. Finally, the paper ends in Section 5.

## 2 More electric system and wing ice protection system (WIPS)

In this section, first, the topology of the multi-electric system is introduced, and then it introduces the design and working principle

of the anti-icing system and de-icing system based on the TFMC; Sections 2.1–2.3 give the layout of heating elements.

### 2.1 More electric system

At present, many large aircraft power distribution systems designs are different voltage levels of AC and DC power supply. There are two voltage classes of DC voltage, 28 and 270 V, in which 28 V is used in aircraft avionics. AC voltage includes two forms, 115 and 230 V, and 230 V is the main distribution network and powered by the starting generators. The design of the MEA distribution system is shown in Fig. 1 [9].

Fig. 1 shows a design of widely used MEA power distribution system, which is composed of two 270 VAC main buses, 'HVAC1' and 'HVAC2'. The main engine (ENG) drives two synchronous generators, SG1 and SG2, respectively, utilising the energy and efficiency supply of the main turbines. The output voltage of these generators is controlled by the generator control units which are similar to the automatic voltage regulators in power system generator controls. The main units on the AC bus are WIPS and the autotransformer rectifier units, which connect two 270 V DC buses to supply power to other DC loads. The DC chopper circuit is used to power the 28 V DC avionics equipment. Besides, there is a basic bus that can be fed from any one of the generators. Electro-mechanical actuators (EMA1 and EMA2) are driven by a permanent magnetic motor. The most important load on the DC bus is the environmental control system that maintains the temperature and pressure of the civilian aircraft. This paper focuses on the design and implementation of WIPS system.

### 2.2 Wing ice protection system

Instead of the traditional pneumatic de-icing system, the TFMC is applied to the WIPS. The utility model has the advantages of saving fuel consumption and improving engine efficiency. The anti-icing and de-icing system of the wing based on the TFMC is shown in Fig. 2.

As shown in Fig. 2, the topology of the TFMC adopts 12 bidirectional switch insulated-gate bipolar transistor (IGBT), which is distributed in a matrix. The three-phase input is 230 VAC voltage, and the output is also three-phase AC voltage. Different from the traditional TFMC, the additional fourth bridge arms,

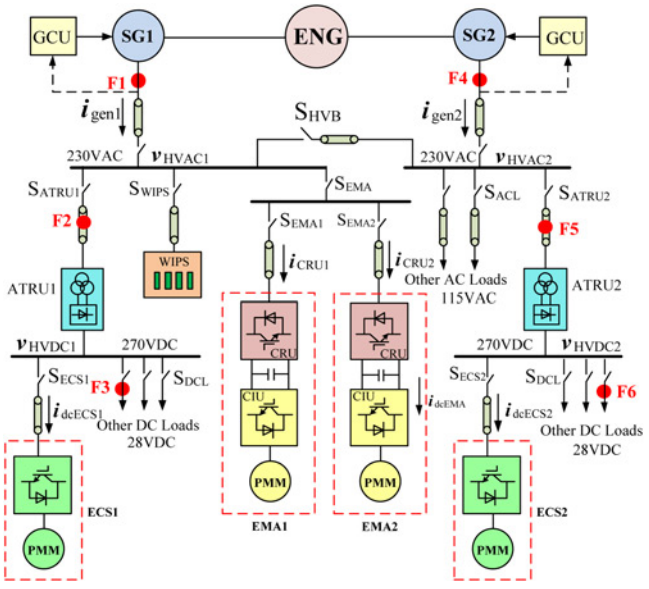


**Fig. 1** *Power distribution system of MEA*

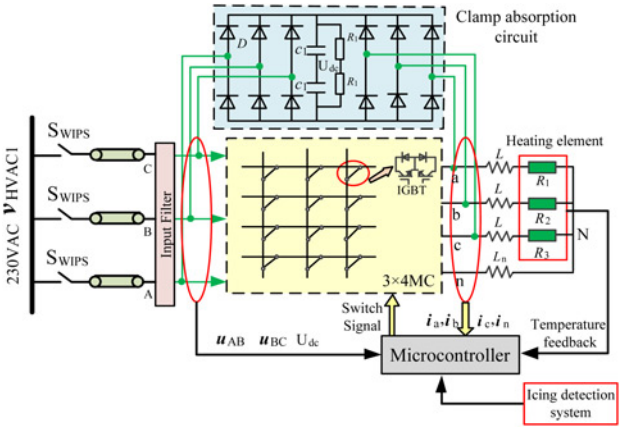


**Fig. 2** *Anti-icing and de-icing system of the wing*

providing access to the zero sequence current as the output load is unbalanced. In order to accomplish the 3DSVM control strategy proposed in this paper, it is necessary to sample three voltage signals and four output current signals. Among them, the $U_{dc}$ is an over-voltage protection signal to protect the safety of the IGBT. The load adopted the heating element mounted on the leading edge slat and the belly, using star connection. According to the signals of the icing detection system and the temperature feedback signal of the heating element, controlling the heating time of the heating element and the heating power, thereby the electric energy is converted into heat energy to prevent the leading edge slat and the belly from freezing. WIPS used a periodic heating method, and stopped when the temperature of the heating element is higher than the preset temperature. The good anti-ice effect is obtained when the heating time is reasonably controlled and energy saving is greatly saved.

### 2.3 Layout of heating elements

The electric heating de-icing system of aircraft usually uses several heating zones. The study found that heating elements that rely on resistance heating can generate hot spots at the centre if the area is large. The partition heating is not only beneficial to the local temperature control of the de-icing thermal load, but also can effectively avoid the central hot spots. Fig. 3 shows a partitioning diagram of the MEA heating pad. Each leading edge slat is divided into six heating zones along the extension direction.

In general, the increase in the number of partitions can reduce the required heating power. However, the partition is increased to a certain number, the effect of energy saving is no longer obvious, and too much partition will cause complex control system and weight increase. It is a complex problem to partition the heating element of the electric heating de-icing heating system in civil aircraft, which needs calculation, analysis and repeated tests.

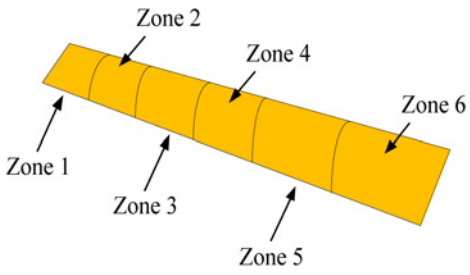


**Fig. 3** *Sketch for MEA thermal mat arrangement*

## 3 3DSVM based on unbalanced loads

According to the Kirchhoff' voltage law (KVL), the sum of the output voltage of the TFMC can be expressed as follows:

$$\boldsymbol{u}_a + \boldsymbol{u}_b + \boldsymbol{u}_c + \boldsymbol{u}_n = \boldsymbol{0} \tag{1}$$

The voltage of any output phase can be represented by other three-phase voltages, as shown in the following equation:

$$\boldsymbol{u}_n = \boldsymbol{u}_a + \boldsymbol{u}_b + \boldsymbol{u}_c \tag{2}$$

The corresponding space vector modulation is transformed from two dimensions into three dimensions.

The TFMC has 81 kinds of switching states. Thirty-six of them produce the rotation voltage vector, which is called 'invalid voltage vectors'. Fourty-five kinds of voltage vectors which produce the fixed direction are called 'effective voltage vectors'. Fig. 4 shows the basic voltage vectors needed to complete the 3DSVM and each desired voltage vector can be synthesised by six basic voltage vectors [10–12].

The time of each switch state can be calculated according to the following equation:

$$\begin{cases} d_1 = \dfrac{2}{\sqrt{3}}\dfrac{|\boldsymbol{V}_d|}{|\boldsymbol{V}_i|}\cos\theta_1\cos\left(\beta_i + \dfrac{\pi}{3}\right) \\ d_2 = \dfrac{2}{\sqrt{3}}\dfrac{|\boldsymbol{V}_d|}{|\boldsymbol{V}_i|}\cos\theta_2\cos\left(\beta_i + \dfrac{\pi}{3}\right) \\ d_3 = \dfrac{2}{\sqrt{3}}\dfrac{|\boldsymbol{V}_d|}{|\boldsymbol{V}_i|}\cos\theta_3\cos\left(\beta_i + \dfrac{\pi}{3}\right) \\ d_4 = \dfrac{2}{\sqrt{3}}\dfrac{|\boldsymbol{V}_d|}{|\boldsymbol{V}_i|}\cos\theta_3\cos\left(\beta_i - \dfrac{\pi}{3}\right) \\ d_5 = \dfrac{2}{\sqrt{3}}\dfrac{|\boldsymbol{V}_d|}{|\boldsymbol{V}_i|}\cos\theta_2\cos\left(\beta_i - \dfrac{\pi}{3}\right) \\ d_6 = \dfrac{2}{\sqrt{3}}\dfrac{|\boldsymbol{V}_d|}{|\boldsymbol{V}_i|}\cos\theta_1\cos\left(\beta_i - \dfrac{\pi}{3}\right) \end{cases} \tag{3}$$

In the above equations, $\theta_1$ represents the angle between the vector $\boldsymbol{V}_2 \times \boldsymbol{V}_3$ and the vector $\boldsymbol{V}_d$, the $\theta_2$, $\theta_3$ also can be calculated in same ways.

When the output three-phase load is asymmetrical, the current is no longer symmetrical. The reason for the three-phase output asymmetrical voltage is that the component of negative and zero sequence in the asymmetrical load current causes a different voltage drop across the load inductor [13]. In the actual modulation algorithm, the output three-phase voltage should be subtracted from this partial voltage drop to obtain the three-phase symmetrical output voltage on the load. The actual output side voltage of the TFMC is given by

$$\begin{aligned} \boldsymbol{u}_{\text{an}} &= U_i\cos(wt) - wLI_a\sin(wt+\theta_a) \\ &\quad - wL_n\left[I_a\sin(wt+\theta_a) + I_b\sin\left(wt - \frac{2\pi}{3} + \theta_b\right)\right. \\ &\quad \left. + I_c\sin\left(wt - \frac{2\pi}{3} + \theta_c\right)\right] \end{aligned} \tag{4}$$

$$\begin{aligned} \boldsymbol{u}_{\text{bn}} &= U_i\cos\left(wt - \frac{2\pi}{3}\right) - wLI_b\sin\left(wt - \frac{2\pi}{3} + \theta_b\right) \\ &\quad - wLn\left[I_a\sin(wt+\theta_a) + I_b\sin(wt - \frac{2\pi}{3} + \theta_b)\right. \\ &\quad \left. + I_c\sin\left(wt + \frac{2\pi}{3} + \theta_c\right)\right] \end{aligned} \tag{5}$$

$$\begin{aligned} \boldsymbol{u}_{\text{cn}} &= U_i\cos\left(wt + \frac{2\pi}{3}\right) - wLI_c\sin\left(wt + \frac{2\pi}{3} + \theta_c\right) \\ &\quad - wLn\left[I_a\sin(wt+\theta_a) + I_b\sin\left(wt - \frac{2\pi}{3} + \theta_b\right)\right. \\ &\quad \left. + I_c\sin\left(wt + \frac{2\pi}{3} + \theta_c\right)\right] \end{aligned} \tag{6}$$

$\theta_a$, $\theta_b$ and $\theta_c$ denote the phase angles of load current. $L$ and $L_n$ denote the output three-phase resistance and fourth leg inductance, respectively.

## 4 Simulation and experimental results

The simulation model of output with unbalanced load based on TFMC is established by using Matlab/Simulink. The simulation parameters are as follows: $U_i = 60$ V, $m = 0.7$, $f_o = 50$ Hz, $f_s = 20$kHz, load inductance $L = 10$ mH, $L_n = 10$ mH, load resistance $R_1 = 10\ \Omega$, $R_2 = 5\ \Omega$, $R_3 = 5\ \Omega$. The parameters input filter are: $L_s = 1$ mH, $C_s = 50\ \mu$F, $R_s = 10\ \Omega$.

The three-phase output voltage and input phase current and voltage are given in Figs. 5 and 6, respectively.

Since the desired output voltage is three-phase symmetrical, the amplitude of the output $a$ phase current is half of the $b$ and $c$ phases. The zero sequence components of current flow in the fourth bridge arm, which is the sine wave. The simulation results satisfy the Kirchhoff current law. Fig. 6 shows that the TFMC satisfies the unit power factor input.

In this paper, a set of highly integrated TFMC experimental platform is developed, which includes input and output modules, bidirectional diode clamp absorption circuit, voltage detection, the current detection module, switch array and IGBT drive module, as shown in Fig. 7.

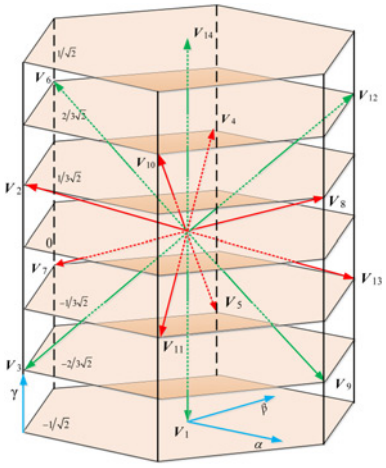


**Fig. 4** *Active voltage vectors based on 3D*

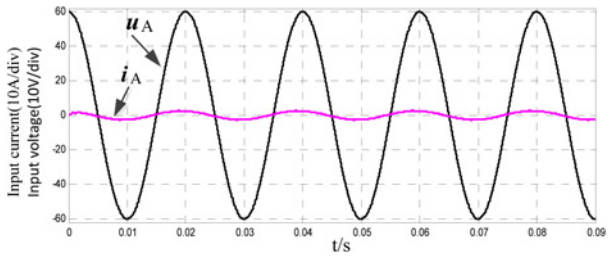


**Fig. 5** *Input current and voltage*

*J. Eng.*, 2018, Vol. 2018, Iss. 13, pp. 529–533
doi: 10.1049/joe.2018.0014

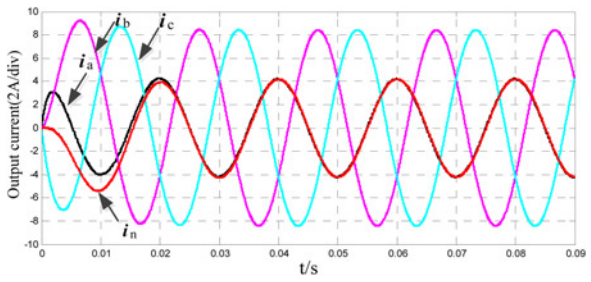


**Fig. 6** *Output current*

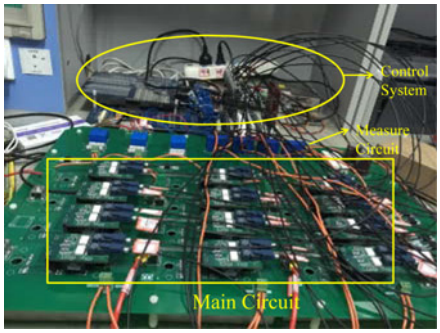


**Fig. 7** *Experimental device of TFMC*

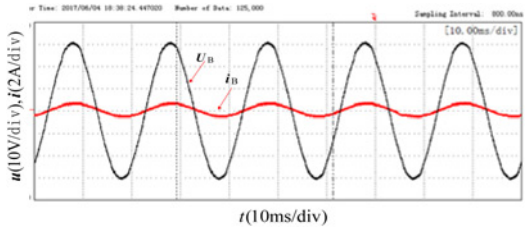


**Fig. 8** *Input current and voltage*

The bidirectional switch used in the experiment is Microsemi's modular switch APTG150DU120TG with switching frequency up to 50 kHz, $V_{CES} = 1200$ V and $I_C = 150$ A. This type of switch has full turn on time of 170 ns, and the full turn off time is 330 ns. In the paper, the switching frequency is set to 5 kHz, input line voltage 40 V, the four-step commutation time 4.2 μs, the output voltage frequency 50 Hz, and other parameters are same as simulation parameters.

The experimental results are shown in Figs. 8 and 9.

From the experiment result shown in Fig. 8, the input voltage and current are basically the same phase and waveform is sinusoidal and symmetrical, satisfying the unit power factor input. From Fig. 9, the waveforms of the output currents $\boldsymbol{i}_a$ and $\boldsymbol{i}_n$ are not completely coincident, and the error is within the acceptable range due to the parameters of the actual circuit, which is not much different from the simulation results. $\boldsymbol{i}_a$, $\boldsymbol{i}_b$ and $\boldsymbol{i}_c$ are sine wave with the phase difference of 120°, and the experimental results are correct. The experiment verifies the correctness of the proposed 3DSVM control strategy by separating the positive, negative zero sequence components of the load current.

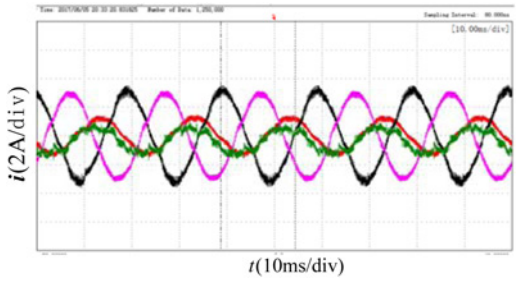


**Fig. 9** *Output current*

It is necessary to point out that the resistance value is the fixed value in the paper. In the actual electrical de-icing system, however, the resistance values can be determined by the icing detection system and sent to the microprocessor as feedback signals. The heating time is determined based on the set actual operating temperature and the temperature of the heating element detected by the detection system.

## 5 Conclusion

In this paper, a set of TFMC based on the WIPS to solve the problem of output with unbalanced load, simulation and experimental verify the correctness of the proposed algorithm. The output power of each of the matrix converter is controlled by detecting the heating element temperature and icing condition in the wing and belly. The key is to reduce the power loss at the abdomen position, saving fuel consumption, which has a bright prospect of engineering application.

## 6 Acknowledgments

This research work has received funding from the National Natural Science Foundation (51677106, 51277156), China Scholarship (201608430006) and Hunan Provincial Innovation Foundation for Postgraduate (CX2017B341). The authors thank many members of the Power Electronics, Machines and Control Group at the Tsinghua University, China.

## 7 References

[1] Cloyd J.S.: 'Status of the United States air force's more electric aircraft initiative', *IEEE Aerosp. Electron. Syst. Mag.*, 1998, **13**, (4), pp. 17–22

[2] Moir I.: 'More-electric aircraft-system considerations'. IEE Colloquium on Electrical Machines and Systems for the More Electric Aircraft, 1999, pp. 1–9

[3] Zhou Q., Nothofer A.: 'Conducted emission analysis of electric nacelle anti ice system in aircraft'. Electrical Systems for Aircraft, Railway and Ship Propulsion, 16–18 October 2012, pp. 1–5

[4] Valasek J.: 'Small unmanned aircraft: theory and practice', *IEEE Electron Device Letters*, 2012, **2**, (4), pp. 103–105

[5] Jones R.I.: 'The more electric aircraft: the past and the future?'. IEE Colloquium on Electrical Machines and Systems for the More Electric Aircraftvol, 1999, pp. 1–4

[6] Sørensen K.L., Helland A.S., Johansen T.A.: 'Carbon nanomaterial-based wing temperature control system for In-flight anti-icing and De-icing of unmanned aerial vehicles'. 2015 IEEE Aerospace Conf., 7–14 March 2015, pp. 1–6

[7] Rosero J.A., Ortega J.A., Aldabas E., *ET AL.*: 'Moving towards a more electric aircraft', *IEEE Aerospace Electron. Syst. Mag.*, 2007, **22**, (3), pp. 3–9

[8] Nothofer A., Tarisciotti L., Zhou Q., *ET AL.*: 'Analysis of conducted emissions from an electric nacelle anti-Ice power control system'. 2016 Int. Symp. on Electromagnetic Compatibility-EMC EUROPE, 5–9 September 2016, pp. 434–439

[9] Wheeler P.: 'Technology for the more and All electric aircraft of the future'. 2016 IEEE Int. Conf. on Automatica (ICA-ACCA), 19–21 October 2016, pp. 1–5

[10] Liu Z., Liu J., Li J.: 'Modelling, analysis, and mitigation of the load neutral point voltage for three-phase four-leg inverter', *IEEE Trans. Ind. Electron.*, 2013, **60**, (5), pp. 2010–2021

[11] Zhang R., Prasd H., Boroyevich D., Lee F.C., *ET AL.*: 'Three-Dimensional space vector modulation for four-Leg voltage-source conveters [J]', *IEEE Trans. Power Electron.*, 2002, **17**, (3), pp. 315–326

[12] Wheeler P.W., Zanchetta P., Clare J., *ET AL.*: 'Utility power supply based on a four-output leg matrix converter [J]', *IEEE Trans. Ind. Electron.*, 2008, **44**, (1), pp. 174–186

[13] Roberto C., Carlos J., Jon C.: 'The application of resonant controllers to four-Leg matrix converters feeding unbalanced or nonlinear loads', *IEEE Trans. Ind. Electron.*, 2012, **27**, (3), pp. 1120–1129